Journal of Histochemistry & Cytochemistry 60(6) 414–427

DOI: 10.1369/0022155412440881
http://jhc.sagepub.com
SAGE

Tropomodulin 1 Constrains Fiber Cell Geometry during Elongation and Maturation in the Lens Cortex

Roberta B. Nowak and Velia M. Fowler
The Scripps Research Institute, La Jolla, California, USA.

Summary

Lens fiber cells exhibit a high degree of hexagonal packing geometry, determined partly by tropomodulin 1 (Tmod1), which stabilizes the spectrin-actin network on lens fiber cell membranes. To ascertain whether Tmod1 is required during epithelial cell differentiation to fiber cells or during fiber cell elongation and maturation, the authors quantified the extent of fiber cell disorder in the Tmod1-null lens and determined locations of disorder by confocal microscopy and computational image analysis. First, nearest neighbor analysis of fiber cell geometry in Tmod1-null lenses showed that disorder is confined to focal patches. Second, differentiating epithelial cells at the equator aligned into ordered meridional rows in Tmod1-null lenses, with disordered patches first observed in elongating fiber cells. Third, as fiber cells were displaced inward in Tmod1-null lenses, total disordered area increased due to increased sizes (but not numbers) of individual disordered patches. The authors conclude that Tmod1 is required first to coordinate fiber cell shapes and interactions during tip migration and elongation and second to stabilize ordered fiber cell geometry during maturation in the lens cortex. An unstable spectrin-actin network without Tmod1 may result in imbalanced forces along membranes, leading to fiber cell rearrangements during elongation, followed by propagation of disorder as fiber cells mature. (J Histochem Cytochem 60:414–427, 2012)

Keywords

ocular lens, hexagonal geometry, tropomodulin, actin, spectrin, membrane skeleton

Lens fiber cells are hexagonally packed to decrease light scattering, a necessity for optical clarity (Tardieu 1988). Fiber cell hexagonal packing arises during differentiation of the short cuboidal lens epithelial cells at the lens equator, where the differentiating cells line up in meridional rows and begin elongating to form fiber cells (Maisel et al. 1981; Lovicu and Robinson 2004). The posterior-most cell of each meridional row becomes a lens fiber cell and elongates until its apical and basal ends reach the poles of the lens. As the lens grows, newly differentiated fiber cells are laid down continuously on top of the elongating fiber cells, forming concentric shells in which fiber cells are packed hexagonally and aligned in radial columns, best evident in cross sections at the lens equator (Kuszak 1995; Bassnett and Winzenburger 2003; Kuszak et al. 2004). The fiber cells in the outermost shell are already hexagonally packed; hence, formation of meridional rows appears to be the order-introducing step in lens packing geometry. This order is conserved as the tips of lens fiber cell cohorts elongate coordinately toward the poles, which can be viewed as a form of collective migration by the cohort of cells in each shell. Hexagonal packing geometry continues to be preserved during fiber cell maturation while shells are successively displaced inward in the lens cortex as a consequence of continuous addition and migration of new shells of younger fiber cells at the periphery. Radial column organization of fiber cells is not perfect. Due to the expansion of the lens circumference during growth, extra columns of fiber cells must be occasionally introduced during differentiation because cell widths do not increase as the lens grows in the mammalian lens, unlike the

Received for publication November 29, 2011; accepted February 8, 2012.

Corresponding Author:
Velia M. Fowler, Department of Cell Biology, CB163, The Scripps Research Institute, 10550 North Torrey Pines Road, La Jolla, CA 92037, USA.
E-mail: velia@scripps.edu

avian lens (Kuszak 1995; Bassnett and Winzenburger 2003; Kuszak et al. 2004). Once fiber cell elongation has completed and the cell tips have reached the anterior and posterior sutures, fiber cells degrade their nuclei and organelles in the inner cortex, eventually forming the organelle-free lens nucleus (Bassnett 2009).

The absence of cell proliferation in the terminally differentiated shells of lens fiber cells contrasts with patterns of hexagonal packing of proliferating cells, in which cell division introduces natural fluctuations in hexagonal packing (Gibson et al. 2006; Farhadifar et al. 2007). Thus, in a randomly dividing cell monolayer, about 45% of cells have six nearest neighbors, defined as cells with a shared membrane boundary. Morphogenetic movements of epithelial sheets, such as convergent extension or intercalation, also lead to variations in the degree of hexagonally packed cells in the absence of cell division (Classen et al. 2005; Blankenship et al. 2006). The percentage of hexagonally packed cells represents the degree of cellular order and can be determined using topological calculations of nearest neighbor analysis in epithelial sheets stained with membrane markers (Classen et al. 2005; Blankenship et al. 2006; Gibson et al. 2006). A higher degree of cellular order, as for lens fiber cells, is thus likely to be the result of active mechanisms imposed during lens epithelial differentiation to fiber cells, followed by their collective elongation toward the poles, and may also necessitate mechanisms to maintain this order as fiber cells mature and age. The synchronous differentiation and elongation of lens fiber cells and the absence of cell division in the terminally differentiated and non-proliferating lens fiber cells thus make them an interesting system to study the initiation and maintenance of hexagonal packing geometry in epithelia.

A structure that influences the morphology and hexagonal packing organization of epithelial cells is the spectrin-based membrane skeleton, originally identified in erythrocytes, where it mediates resistance to forces in the bloodstream (Mohandas and Evans 1994; Bennett and Baines 2001). The membrane skeleton is a network of spectrin tetramers cross-linked by short actin filament (F-actin) linkers that are attached to adhesion receptors, ion pumps, and channels via linkage of spectrin to ankyrins and other adaptors (Luna and Hitt 1992; Bennett and Baines 2001; Dubreuil 2006; Bennett and Healy 2008). The short F-actin linkers form structural nodes in this network and are capped by adducin at their barbed ends and tropomodulin 1 (Tmod1) at their pointed ends (Fowler 1987; Gilligan and Bennett 1993; Fowler 1996; Kuhlman et al. 1996). Tropomyosin is also bound along the short F-actin linkers and is stabilized on actin by interaction with Tmod1 (Fowler and Bennett 1984; Weber A et al. 1994). The absence of Tmod1 in erythrocytes leads to F-actin instability with misregulated filament lengths and a disrupted membrane skeleton, resulting in a mild, compensated sphero-elliptocytic anemia with osmotically fragile and misshapen cells (Moyer et al. 2010). In cultured epithelial cells, F-actin stability mediated by Tmods and adducins (Weber KL et al. 2007; Abdi and Bennett 2008), as well as attachment of spectrin to the membrane via ankyrins, is important for normal cell morphology and hexagonal packing (Kizhatil and Bennett 2004; Kizhatil, Davis, et al. 2007; Kizhatil, Yoon, et al. 2007).

Recently, we have shown that absence of Tmod1 in fiber cells of the mouse lens leads to reduced levels of a γTM isoform, F-actin disassembly, and disruption of the spectrin-actin network, accompanied by perturbed radial column organization with patches of disordered fiber cells in the lens cortex (Nowak et al. 2009). Fiber cell membranes also display abnormal protrusions and membrane morphologies in the absence of Tmod1, indicative of altered fiber cell-cell interactions and disordered packing. However, it was not clear from this study whether the disordered fiber cell patches in the Tmod1-null lens appeared during epithelial cell differentiation to fiber cells or, alternatively, during subsequent fiber cell elongation and/or maturation. Namely, is fiber cell disorder in the absence of Tmod1 due to a failure to establish ordered hexagonal packing early during epithelial cell differentiation to fiber cells or to a failure to maintain packing during subsequent fiber cell elongation and maturation?

Our data show that in the absence of Tmod1, fiber cell disorder was not apparent during epithelial cell differentiation when hexagonal packing was first established in the meridional rows at the equator. Instead, disordered patches of fiber cells first appeared in Tmod1-null young elongating fiber cells located adjacent to the epithelium near the equator. Unexpectedly, as fiber cells matured without Tmod1, the numbers of disordered patches did not appear to increase significantly, but the total disordered area was substantially higher due to significantly larger sizes of individual disordered patches. Loss of hexagonal packing geometry in the absence of Tmod1 was restricted exclusively to these patches, based on quantitative nearest neighbor analysis of cells in disordered patches or adjacent regions displaying normal radial column alignment. We propose that absence of Tmod1 leads to insufficient reinforcement of the spectrin-actin network, leading to network disruptions and failure to maintain fiber cell interactions and hexagonal geometry during collective fiber cell migration and elongation, as well as during fiber cell maturation in the cortex. We present a mechanism explaining how small packing defects can appear and enlarge under the influence of non-uniform physical stresses in the lens, giving rise to higher disorder in the presence of a weakened spectrin-actin lattice.

Materials and Methods

Mouse Strain

Tmod1$^{-/-Tg^{+}}$ mice have been described previously (McKeown et al. 2008). In this strain, the embryonic lethality of the

Tmod1–/– mouse (Fritz-Six et al. 2003) was rescued by expression of a Tmod1-overexpressing transgene in the heart under the control of the cardiac-specific α-myosin heavy chain (α-MHC) promoter (*Tg(αMHC-Tmod1)*, referred to as *Tg*+). *Tmod1*+/+ $^{Tg+}$ animals expressing the α-MHC-Tmod1 transgene in their heart had normal levels of Tmod1 in all tissues except the heart, whereas *Tmod1–/–*$^{Tg+}$ animals had no Tmod1 in any tissues except the heart (McKeown et al. 2008; Nowak et al. 2009; Gokhin et al. 2010; Moyer et al. 2010). The *Tg(αMHC-Tmod1)* mice were generated on an FVB/N background (Sussman et al. 1998), which has an endogenous mutation in the *Bfsp2/CP49* gene (Simirskii et al. 2006). Thus, lenses from both *Tmod1*+/+$^{Tg+}$ and *Tmod1–/–*$^{Tg+}$ mice are missing the beaded filament protein, CP49, and have reduced levels of filensin, as shown previously (Nowak et al. 2009). Animals were all 1 month old at the time of sacrifice. All procedures were performed in accordance with The Scripps Research Institute animal care guidelines.

Lens Sectioning and Staining

Eyes were dissected out of the mice, cut open at the posterior to allow entry of the fixative, and fixed in either 1% paraformaldehyde in PBS overnight at 4C (for F-actin staining) or 0.75% paraformaldehyde in PBS for 4 hr at room temperature (for antibody plus F-actin staining) (Nowak et al. 2009). Eyes were washed three times for 10 min in PBS. Subsequently, eyes were immersed in a sucrose gradient, first 10% sucrose for 1 hr at room temperature, then 20% sucrose for 1 hr at room temperature, and finally 40% sucrose overnight at 4C. After this treatment, both eyes of each mouse were incubated in OCT (Sakura Finetek; Torrance, CA) for 30 min and frozen in OCT with eyes oriented in the equatorial plane for sectioning. Blocks were stored at −80C. Then, 14-μm sections were prepared with a cryostat (Leica CM1950) and melted on ColorFrost Plus glass slides (Fisher Scientific; Pittsburgh, PA). Slides were either stained directly or stored at −20C for a maximum of 2 weeks before staining.

For staining of slides stored at −20C, slides were thawed and air-dried for 20 min. Subsequently, slides were washed with PBS containing 0.1% Triton X-100 (PBST) for 20 min and permeabilized for 25 min with PBS containing 0.3% Triton X-100. Slides were blocked with PBST supplemented with 3% BSA and 1% goat serum followed by staining for F-actin overnight at 4C in blocking solution in a humidified chamber, using Alexa 647–phalloidin or rhodamine-phalloidin (1:200; Molecular Probes, Carlsbad, CA). In some experiments, membranes were stained with Alexa 555–conjugated wheat germ agglutinin (WGA) (2 μg/ml; Molecular Probes) or a rat polyclonal against N-cadherin (1:10; Developmental Studies Hybridoma Bank [DHSB], Iowa City, IA). Tmod1 was stained with affinity-purified rabbit antibodies to human Tmod1 (R1749) (2 μg/ml). After staining with primary antibodies, slides were washed three times for 10 min in PBST, followed by incubation for 1 hr at room temperature with appropriate secondary antibodies supplemented with phalloidin. Subsequently, slides were again washed three times for 10 min and mounted using Gel/Mount (Biomeda, Foster City, CA). Secondary antibodies used were Alexa 647–conjugated goat–anti-mouse (1:200; Molecular Probes), Alexa 488–conjugated goat–anti-rat (1:200; Molecular Probes), or Alexa 488–conjugated goat–anti-rabbit (1:200; Molecular Probes).

For whole-mount imaging experiments, freshly dissected lenses were incubated in M199 medium (Invitrogen; Carlsbad, CA) supplemented with Hoechst (1:500; Sigma, St. Louis, MO) for 1 hr at 37C to stain nuclei. Whole lenses were placed on their sides in the well of a glass-bottomed dish (MatTek Corp.; Ashland, MA) in Dulbecco's PBS (Invitrogen) to image the nuclei of the epithelial cells and the differentiating fiber cells at the equator.

Imaging and Quantitative Image Analysis

Images were acquired using a Bio-Rad (Hercules, CA) Radiance 2100 laser-scanning confocal microscope. Images of lens cryosections for fiber cell nearest neighbor analysis were acquired using a 100×/1.4 N.A. objective. Images of lens cryosections for disordered area measurements and stacks of whole-mount lenses were acquired using a 20×/0.75 N.A. objective. The Z-step size for stacks was 2 μm, with each slice being 2 μm thick. Images were analyzed using Volocity 4 (Improvision; Waltham, MA) and ImageJ (http://rsbweb.nih.gov/ij).

The procedure for fiber cell nearest neighbor analysis for lens cryosections was based on methods developed for analysis of simple epithelial cell sheets (Classen et al. 2005; Farhadifar et al. 2007), with modifications as follows. Because the accuracy of the final computational analysis depends on reliable image segmentation to clearly identify membrane boundaries, a series of membrane-associated stains (WGA, N-cadherin, F-actin) were evaluated first, revealing that rhodamine-phalloidin staining for F-actin provided the most reliable membrane marker for these computational analyses. WGA was not optimal because it stained the nuclear envelope in addition to the plasma membrane, which is problematic for the thin lens fiber cells in which the plasma membranes often contact the nuclear envelope, leading to incorrect delineation of cell boundaries. N-cadherin was not optimal due to somewhat high cytoplasmic staining in young fiber cells, along with a punctate and relatively weak staining of fiber cell broad sides, which resulted in gaps in the membranes, also leading to incorrect delineation of cell boundaries (data not shown). On other hand, F-actin staining outlined the plasma membrane with a relatively good membrane/cytoplasm contrast in all fiber cells, and furthermore, phalloidin could stain F-actin in

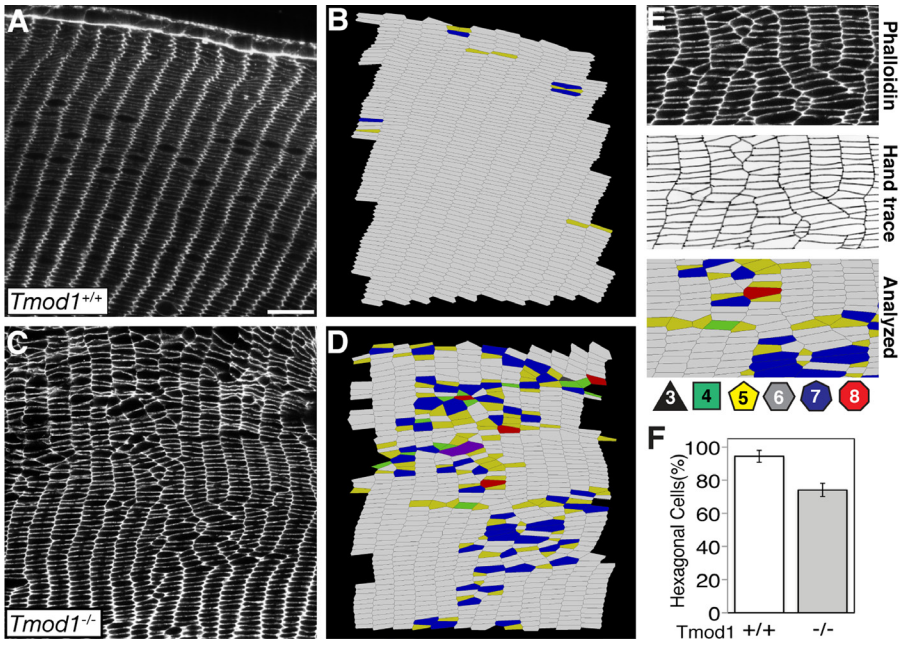

Figure 1. Hexagonal packing of fiber cells is reduced in regions of *Tmod1–/–*$^{Tg+}$ lenses with misaligned radial columns. (A, C) Equatorial sections of 1-month-old mouse lenses stained for F-actin showing well-aligned radial columns in *Tmod1*+/+$^{Tg+}$ lenses (A) but misaligned fiber cells with radial column branching in *Tmod1–/–*$^{Tg+}$ lenses (C). Bar, 18 µm. (B, D) Nearest neighbor analysis of images in A, C showing that fiber cells with six nearest neighbors (gray) predominate in *Tmod1*+/+$^{Tg+}$ lenses, but disordered patches containing many fiber cells with less than or more than six nearest neighbors are found in *Tmod1–/–*$^{Tg+}$ lenses (colors). (E) Enlargement illustrating the variety of packing deviations in disordered patches in *Tmod1–/–*$^{Tg+}$ lenses. Top, phalloidin staining for F-actin; Middle, cell boundaries traced from phalloidin staining; Bottom, cells colored according to numbers of nearest neighbors. Color code: cells with three (black), four (green), five (yellow), six (gray), seven (blue), and eight (red) nearest neighbors. (F) Quantification reveals that ~90% of fiber cells have six nearest neighbors in *Tmod1*+/+$^{Tg+}$ lenses, as compared with ~74% of fiber cells with six nearest neighbors in regions with misaligned radial columns in *Tmod1–/–*$^{Tg+}$ lenses ($p<0.05$). $n = 3$ images from three lenses per genotype. Error bars, SD.

lenses that had been fixed more extensively, thus providing better preservation of fiber cell geometry.

Next, we compared an automated image segmentation approach to delineate fiber cell boundaries with a manual outlining procedure using transparency film. The latter was more accurate and more efficient for lens fiber cells because of the very flattened hexagonal shapes of lens fiber cells, compounded by the fragility and distortions inherent in lens cryosections, which often led to collapse of cell membranes upon one another. A transparency film was placed over a printout of each fluorescent image, and fiber cell boundaries were outlined with a marker. Transparency films were scanned at 300 dpi and analyzed for nearest neighbors using PackingAnalyzer 1.0 (http://idisk-srv1.mpi-cbg.de/~eaton). Statistical analysis was performed using Excel (Microsoft Corp.; Redmond, WA) and R (hppt://www.r-project.org). If not stated otherwise, Student's *t*-test was used for statistical analysis. Statistical significance was defined as $p<0.05$.

Results

Fiber cells exhibit reduced hexagonal packing only in regions with branched radial columns in Tmod1-null lenses. Previously, we identified patches of disordered fiber cells in the cortex of *Tmod1–/–*$^{Tg+}$ (but not *Tmod1*+/+$^{Tg+}$) lenses by visual inspection of equatorial cryosections from 1-month-old lenses (Nowak et al. 2009). In that study, fiber cell disorder in adult lenses was quantified by tracing radial cell columns and counting branches between two neighboring columns. Although aligned radial columns are a necessary result of hexagonal packing, and radial column branching is associated with disrupted hexagonal packing, our analysis did not address directly to what extent hexagonal packing was altered in *Tmod1–/–*$^{Tg+}$ lenses. To evaluate this, we stained equatorial cryosections of 1-month-old lenses with rhodamine-phalloidin to outline fiber cell membranes and used a computational image analysis method to determine the numbers of nearest neighbors for each fiber cell (Fig. 1E; see Materials and Methods). In wild-type lenses where radial columns are well aligned (Fig. 1A), nearest neighbor analysis of cortical fiber cells within ~100 microns of the epithelium reveals that more than 90% to 95% of fiber cells are hexagonally packed (i.e., with six nearest neighbors) (Fig. 1B, F). Occasional small packing imperfections are observed involving around two to six adjacent fiber cells, due mostly to small alignment shifts at short membrane sides (Fig. 1B, yellow and blue cells; also see Fig. 2C). In contrast, the regions with branched radial columns in *Tmod1–/–*$^{Tg+}$ lenses (Fig. 1C) typically display large disordered patches where many adjacent fiber cells have from four to eight nearest neighbors (Fig. 1D,E). Quantitative analysis reveals that only ~70% of fiber cells are hexagonally packed (i.e., with six nearest neighbors) in the regions of *Tmod1–/–*$^{Tg+}$ lenses with branched radial columns (Fig. 1F).

Next, we selected regions of *Tmod1–/–*$^{Tg+}$ lenses with unbranched radial columns to investigate whether subtle

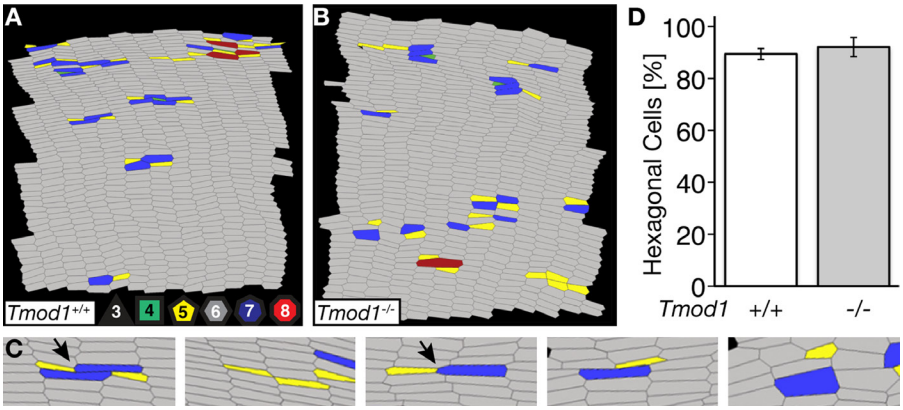

Figure 2. Fiber cells are hexagonally packed in regions with aligned radial columns in both *Tmod1*+/+$^{Tg+}$ and *Tmod1*–/–$^{Tg+}$ lenses. (A, B) Nearest neighbor analysis of images of equatorial sections of 1-month-old mouse lenses stained for F-actin (not shown), showing that most cells from either *Tmod1*+/+$^{Tg+}$ (left) or *Tmod1*–/–$^{Tg+}$ (right) lenses have six nearest neighbors (gray), whereas only small patches (around two to eight cells) have less than or more than six neighbors (colors). Color code: cells with three (black), four (green), five (yellow), six (gray), seven (blue), and eight (red) nearest neighbors. (C) Enlargement illustrating examples of small local packing defects observed in aligned areas of either genotype. Cells from one radial column can intrude slightly into another column, leading to altered numbers of nearest neighbors, or to a slight offset between adjacent radial columns (arrows), but without affecting overall radial column alignment. (D) Quantification shows that ~90% of fiber cells have six nearest neighbors in regions with normal radial column alignment in both *Tmod1*+/+$^{Tg+}$ and *Tmod1*–/–$^{Tg+}$ lenses (p=0.13). n=2–3 images from three lenses per genotype. Error bars, SD.

defects in fiber cell packing might also be present in these regions. Visual comparison of nearest neighbors in such relatively well-ordered regions of wild-type and *Tmod1*–/–$^{Tg+}$ lenses reveals only minor packing imperfections, with small groups of fiber cells displaying from four to seven nearest neighbors (Fig. 2A–C). However, quantitative analysis of nearest neighbors establishes that ~90% of fiber cells were hexagonally packed in the regions of *Tmod1*–/–$^{Tg+}$ lenses with unbranched radial columns, similar to the *Tmod1*+/+$^{Tg+}$ lenses (Fig. 2D). It is worth noting that the small packing imperfections found in these unbranched regions (i.e., outside the large disordered fiber cell patches) occurred in both *Tmod1*+/+$^{Tg+}$ and *Tmod1*–/–$^{Tg+}$ lenses alike (Fig. 2A,B; enlargements of small packing imperfections shown in Fig. 2C). Some of these small packing imperfections may be due to fiber cell fusions or to radial column branching during addition of new fiber cells during lens growth (Kuszak et al. 2004; Shi et al. 2009), but these events are unlikely to account for all of the small packing imperfections we observe. Instead, many packing imperfections are likely a consequence of the extremely flattened hexagonal shape of fiber cells, resulting in an inability to distinguish the two neighboring vertices at fiber cell short sides, owing to small distortions inherent to the cryosectioning process (Fig. 2C). In our procedure, if two vertices could not be discerned they were counted as one, necessarily leading to altered numbers of nearest neighbors and non-hexagonal packing imperfections. Some of these events are surely artifactual, hence underestimating the real degree of hexagonal packing. In conclusion, regions with branching radial cell columns in *Tmod1*–/–$^{Tg+}$ lenses contain misaligned fiber cells forming disordered patches, with a ~20% decrease in hexagonal packing, supporting our previous qualitative observations (Nowak et al. 2009). However, decreased hexagonal packing in the absence of Tmod1 is restricted to these regions, and there is no global change in hexagonal packing outside of these patches, allowing us to limit our further analysis exclusively to disordered patches in regions with radial column branching.

Higher disorder in Tmod1-null lenses is not caused by failure to establish epithelial cell alignment into meridional rows at the equator. One possible mechanism to account for the appearance of disordered patches of fiber cells in the lens cortex could be that initial establishment of hexagonal packing is perturbed in *Tmod1*–/–$^{Tg+}$ lenses. In mammalian lenses, randomly oriented epithelial cells covering the anterior side of the lens line up at the equator to form meridional rows before they terminally differentiate into lens fiber cells (Maisel et al. 1981; Lovicu and Robinson 2004). As epithelial cells are proliferating before they enter the process of fiber cell differentiation, failure to synchronously exit the cell cycle, polarize, and coordinately align in meridional rows could lead to disordered cellular packing. Misalignment of epithelial cells in the meridional rows could be perpetuated during fiber cell elongation, hence leading to disordered packing geometries of lens fiber cells as they mature in the cortex. To investigate this possibility, we evaluated epithelial cell alignment at the lens equator by Hoechst staining of nuclei in whole mounts of lenses, followed by confocal fluorescence microscopy. Lenses were oriented on their sides to image the equatorial region, and a three-dimensional reconstruction of a Z stack was performed and reoriented to visualize en face the meridional rows and adjacent anterior epithelial cells (Fig. 3). Epithelial cells anterior to the meridional rows are randomly oriented, and the anterior-most cells at the tops of the meridional rows are next in line to begin differentiating into lens fiber cells. Note that the fiber cell nuclei are not visible in

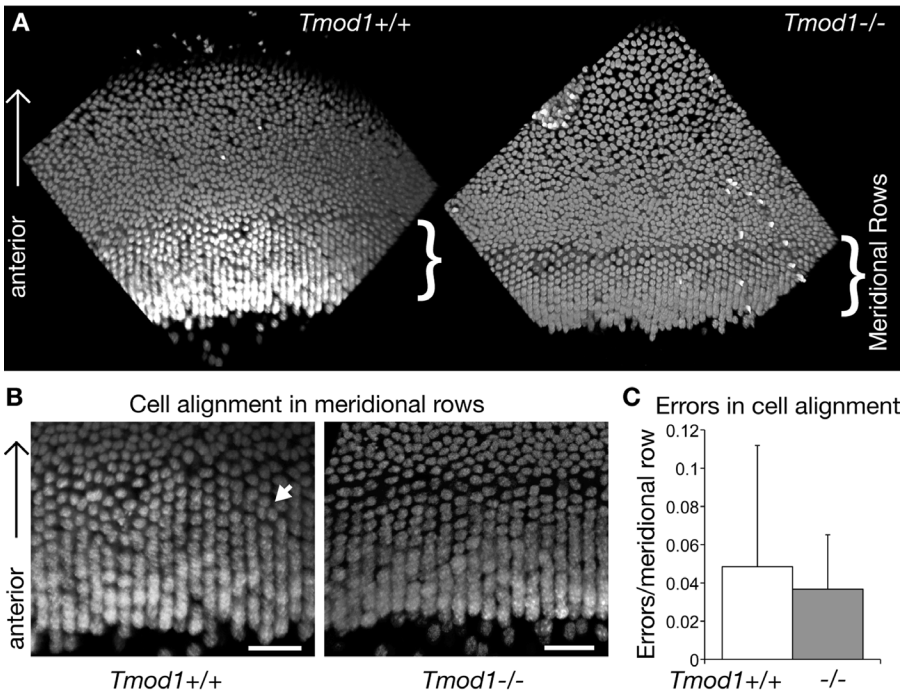

Figure 3. Epithelial cell alignment in meridional rows at the equator is similar in *Tmod1*+/+$^{Tg+}$ and *Tmod1*–/–$^{Tg+}$ lenses. (A) Three-dimensional reconstructions of confocal stacks from Hoechst-stained nuclei of equatorial epithelial cells in lens whole mounts. In 1-month-old mice, about 10 to 12 lens epithelial cells align to form meridional rows (brackets) before differentiating and elongating into fiber cells at the equator. (B) In higher magnification images,alignment of nuclei into vertical rows appears qualitatively similar in both genotypes. Arrow, alignment defect with a misplaced nucleus. Bars = 20 μm. (C) Quantification of alignment errors per row shows no significant difference in alignment fidelity between *Tmod1*+/+$^{Tg+}$ and *Tmod1*–/–$^{Tg+}$ lenses (p=0.75). n = 425 and 401 rows total from one to two confocal stacks per lens, for three *Tmod1*+/+$^{Tg+}$ and three *Tmod1*–/–$^{Tg+}$ lenses, respectively. Error bars, SD.

these images because as the cells begin to elongate, they curve, and the nuclei move out of the optical section at the bottom of the images.

Analysis of three-dimensional image reconstructions from confocal stacks showed that in 1-month-old mice, about 10 to 12 epithelial cells are aligned in vertical rows just anterior to the equator in both *Tmod1*+/+$^{Tg+}$ and *Tmod1*–/–$^{Tg+}$ lenses (Fig. 3A, brackets). The number of cells aligned in meridional rows is lower in older mice of both genotypes (data not shown), due to the slower rate of epithelial-to-fiber cell differentiation and slower rate of lens growth (Shui and Beebe 2008). No overall morphological differences in the arrangement of Hoechst-stained nuclei in this region are observed between *Tmod1*+/+$^{Tg+}$ and *Tmod1*–/–$^{Tg+}$ mice (Fig. 3A,B). Quantitative analysis of alignment defects in higher magnification images of meridional rows was carried out by counting misplaced nuclei—for example, two nuclei located in the place of one, or a nucleus not aligned with others located in the same row (Fig. 3B, arrow). After normalization of the number of alignment defects relative to the number of meridional rows counted for each genotype, no significant differences in numbers of alignment defects were observed between *Tmod1*+/+$^{Tg+}$ and *Tmod1*–/–$^{Tg+}$ lenses (Fig. 3C). These data indicate that the alignment of epithelial cells into meridional rows is unchanged in *Tmod1*–/–$^{Tg+}$ lenses and thus does not appear to account for the decreased hexagonal packing of cortical fiber cells observed in these lenses.

Disordered patches first appear in elongating fiber cells near the epithelium in the absence of Tmod1 and increase in number and size as fiber cells mature. Because initial epithelial cell differentiation and packing organization are not affected by the absence of Tmod1, we hypothesized that fiber cell disorder in *Tmod1*–/–$^{Tg+}$ lenses may appear subsequently during fiber cell elongation and/or maturation. Because new fiber cells are added to the periphery of the lens during growth, the distance of fiber cells from the epithelium reflects their increasing maturity. Our previous work had shown that Tmod1 levels increased greatly in cells located about 40 to 50 μm in from the epithelium, suggesting the hypothesis that fiber cell disorder might appear in this region due to destabilization of the spectrin-actin network in maturing fiber cells in the absence of Tmod1 (Nowak et al. 2009). Therefore, to assess this possibility, we set out to quantify the amount of disorder in *Tmod1*–/–$^{Tg+}$ lenses with respect to fiber cell radial location inside the lens. For these experiments, low-magnification images of equatorial cryosections double-stained for Tmod1 and F-actin were obtained by confocal microscopy to visualize young cortical fiber cells located near the epithelium, as well as older maturing cells located up to ~250 μm away from the epithelium, toward the center of the lens (Fig. 4A–F). In *Tmod1*+/+$^{Tg+}$ lenses, these low-magnification images reveal intense, crisp F-actin staining on fiber cell vertices all the way from the epithelium to the inner fiber cells of the cortex, delineating the radial columns, as expected (Fig. 4B,C). However, for unexplained reasons, the F-actin staining quality in *Tmod1*–/–$^{Tg+}$

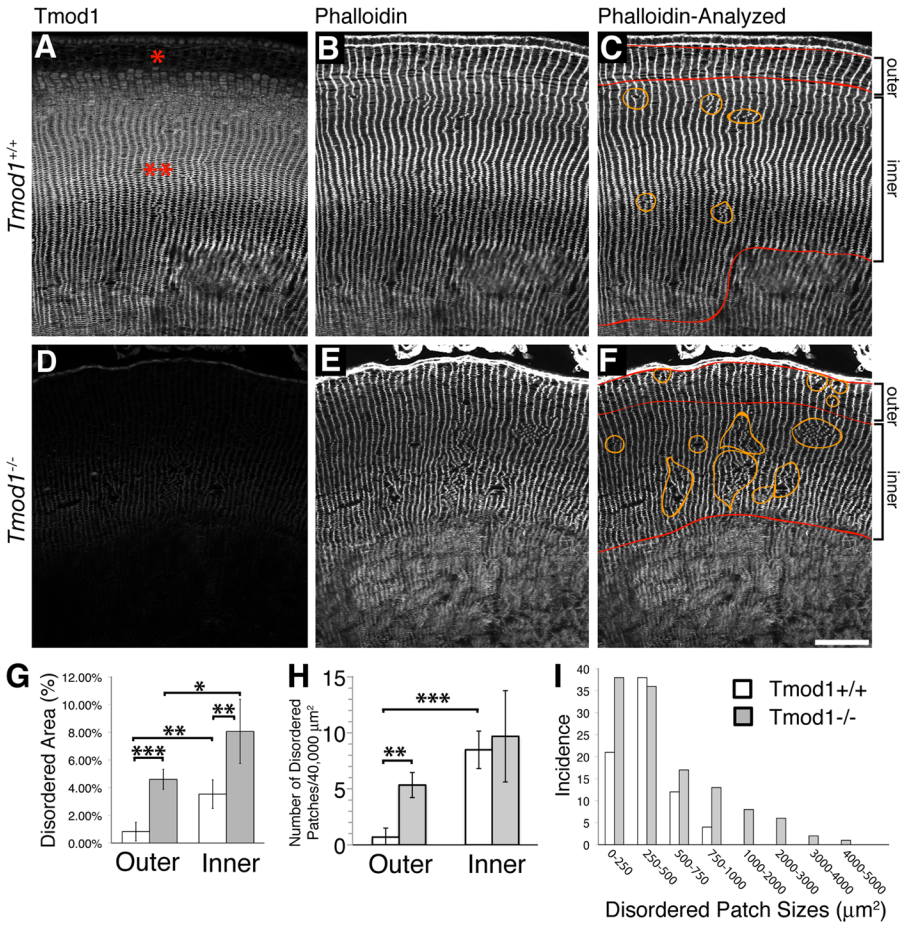

Figure 4. The total area of fiber cell disorder is greater in the *Tmod1*–/–$^{Tg+}$ lens cortex, with more numerous and larger disordered patches, as compared with the *Tmod1*+/+$^{Tg+}$ lens cortex. (A–F) Low-magnification images of equatorial sections of 1-month-old lenses stained for Tmod1 (A, D) and F-actin (B, E) to reveal radial column organization. (A) Tmod1 staining in *Tmod1*+/+$^{Tg+}$ lenses is low in the outer region located up to ~50 µm from the epithelium (red asterisk) and increases greatly in the inner region located between ~50 and ~250 µm from the epithelium (double red asterisks). (C, F) Areas with disrupted radial columns, indicated by discontinuities in F-actin vertical stripes, are outlined with orange lines. The horizontal red lines indicate the outer region (0 to ~50 µm from the epithelium) and inner region (~50 to ~250 µm from the epithelium) where disorder was measured. (E) Note that poor F-actin staining in the inner cortex of *Tmod1*–/–$^{Tg+}$ lenses reduced the depth of the measurable inner region to ~150 µm from the epithelium. (G) Percentage of disordered area in outer and inner regions. The sum of individual areas was normalized to the total area analyzed for each image and region and expressed as a percentage. (H) Numbers of individual disordered patches in the outer and inner regions, normalized to the µm^2 measured. (I) Sizes of individual disordered patches, grouped in the size classes indicated. n=6 sections from four *Tmod1*+/+$^{Tg+}$ lenses (two mice) and n = 5 sections from four *Tmod1*–/–$^{Tg+}$ lenses (two mice). Error bars, SD. *p<0.05. **p<0.001. ***p<0.0001.

lenses consistently deteriorated at ~100 to 150 µm away from the epithelium in the inner cortex, thus reducing the measurable area (Fig. 4E,F). Disordered areas of fiber cells were identified based on obvious discontinuities in F-actin staining along radial columns, areas were outlined manually using Image J (National Institutes of Health) (Fig. 4C,F, orange lines), and percentages of total disordered areas, as well as individual numbers and sizes of disordered patches, were measured (Fig. 4G–I). In addition, the cortex was divided into two regions: a thin outer region defined by low Tmod1 staining (0 to ~50 µm) and a broad inner region more distant from the epithelium, with increased Tmod1 staining (~50 to ~250 µm) (Fig. 4A, asterisks; Fig. 4C,F, red lines). All measurements were normalized to the total image area measured in each sample.

To our surprise, in the outer region where Tmod1 staining is low in *Tmod1*+/+$^{Tg+}$ lenses, the percentage of disordered area in *Tmod1*–/–$^{Tg+}$ lenses was ~5-fold greater than in the *Tmod1*+/+$^{Tg+}$ lenses (p<0.0001) (Fig. 4G). In the inner region, where Tmod1 levels are elevated in *Tmod1*+/+$^{Tg+}$ lenses, the percentage of disordered area was increased significantly for both genotypes, but the total disordered area was ~2-fold greater in *Tmod1*–/–$^{Tg+}$ compared with *Tmod1*+/+$^{Tg+}$ lenses (p<0.001) (Fig. 4G). Furthermore, in the outer region, the numbers of individual disordered patches were ~8-fold greater for *Tmod1*–/–$^{Tg+}$ than for *Tmod1*+/+$^{Tg+}$ lenses, which had negligible numbers of disordered patches in the outer region (p<0.001) (Fig. 4H).

Next, we compared the numbers of disordered patches in the inner and outer regions and found that the numbers of disordered patches increased in *Tmod1*+/+$^{Tg+}$ lenses but not in *Tmod1*–/–$^{Tg+}$ lenses, resulting in similar numbers of disordered patches in the inner regions in both genotypes (Fig. 4H). Nevertheless, the total disordered area was

significantly greater in *Tmod1*–/–$^{Tg+}$ as compared with *Tmod1*+/+$^{Tg+}$ lenses (Fig. 4G). To investigate whether this could be due to larger patch sizes in *Tmod1*–/–$^{Tg+}$ lenses, we measured sizes of individual disordered patches for each genotype. We classified disordered patches according to their size and grouped patches into size classes of ~250 μm^2. Analysis of the resulting size distributions revealed that most disordered patches in *Tmod1*+/+$^{Tg+}$ lenses are between 250 and 500 μm^2, whereas disordered patches larger than 500 μm^2 predominate in *Tmod1*–/–$^{Tg+}$ lenses, with especially large disordered patches of fiber cells (>1000 μm^2) observed frequently in *Tmod1*–/–$^{Tg+}$ lenses but never in *Tmod1*+/+$^{Tg+}$ lenses (Fig. 4I). A Student's *t*-test confirms that individual disordered patches of fiber cells are significantly larger in the absence of Tmod1 (p=1.5 × 10^{-8}). Therefore, in the region between ~50 and 200 μm inward from the epithelium, the higher degree of disorder in *Tmod1*–/–$^{Tg+}$ lenses as compared with *Tmod1*+/+$^{Tg+}$ lenses is due to larger sizes of individual disordered patches in the absence of Tmod1.

In conclusion, these results show, first, that disordered patches in *Tmod1*–/–$^{Tg+}$ lenses appear initially in the fiber cells adjacent to the epithelium at the equator, thus appearing in young, elongating fiber cells. Second, the greater overall percentage of disorder in *Tmod1*–/–$^{Tg+}$ lenses compared with *Tmod1*+/+$^{Tg+}$ lenses is due to increased numbers of disordered patches in the outer region, together with increased sizes of disordered patches in the inner region in the absence of Tmod1. Third, the amount of disordered area depends on radial location in the lens, increasing in older fiber cells located from ~50 to ~200 μm in from the epithelium, for both *Tmod1*+/+$^{Tg+}$ and *Tmod1*–/–$^{Tg+}$ lenses. For *Tmod1*+/+$^{Tg+}$ lenses, this increase in disorder represents the appearance of new but small disordered patches, whereas for *Tmod1*–/–$^{Tg+}$ lenses, this predominantly represents greater sizes of existing patches. This suggests that once disordered patches form, disorder is propagated so that the patches tend to grow in size in *Tmod1*–/–$^{Tg+}$ but not *Tmod1*+/+$^{Tg+}$ lenses.

Tmod1 protein is detected in young fiber cells near the epithelium, where F-actin organization is less uniform on fiber cell membranes. The appearance of disordered packing in young fiber cells adjacent to the epithelium of *Tmod1*–/–$^{Tg+}$ lenses suggests that Tmod1 is required to maintain fiber cell organization during coordinated fiber cell tip elongation and migration toward the poles. This was unexpected based on our previous observations that Tmod1 staining was barely detectable in young fiber cells near the equator (Nowak et al. 2009). Therefore, we reevaluated the presence of Tmod1 in the young, elongating fiber cells by reexamining Tmod1 staining in high-magnification confocal image stacks of *Tmod1*+/+$^{Tg+}$ and *Tmod1*–/–$^{Tg+}$ lens sections (Fig. 5). The equatorial region containing the young fiber cells was identified from serial sections based on the height of the epithelium, selecting the sections with the tallest epithelium. We then zeroed in on this region at high magnification so that the markedly higher levels of Tmod1 signal in the older fiber cells located further inward would not obscure the lower signal intensity in these young cells (as likely happened in our previous study) (Nowak et al. 2009). Comparison of Tmod1 staining between *Tmod1*+/+$^{Tg+}$ and *Tmod1*–/–$^{Tg+}$ lenses demonstrates that Tmod1 staining is detected in the young fiber cells from *Tmod1*+/+$^{Tg+}$ (Fig. 5A,C) but not *Tmod1*–/–$^{Tg+}$ lenses (Fig. 5D,F). Note that the epithelial and fiber cell nuclei are stained nonspecifically in the *Tmod1*–/–$^{Tg+}$ lenses (Fig. 5D, asterisks), as reported previously (Nowak et al. 2009). Furthermore, Tmod1 staining is clearly concentrated on the broad sides of the fiber cell membranes (Fig. 5A,C), with a lower signal at the vertices; this is opposite to F-actin, which is more intense at the vertices (Fig. 5B,C), as shown before (Nowak et al. 2009). Previously, in somewhat older fiber cells, we had localized Tmod1 to both the broad and narrow sides (Nowak et al. 2009). Although the extreme thinness of the young fiber cells makes it impossible to resolve the narrow sides from the vertices in the three-dimensional images of the confocal stacks, single optical sections of lens cryosections that have been mechanically stretched during cryosectioning reveal that F-actin is enriched at the vertices, whereas Tmod1 is on both short and long sides (see Fig. 2P-S in Nowak et al. 2009). The peripheral fiber cells shown here in Figure 1A also demonstrate F-actin on short sides and vertices, with preferential enrichment of F-actin at the vertices. Therefore, we conclude that Tmod1 is indeed present in young, elongating fiber cells at the equator, where it is associated with fiber cell membranes, thus plausibly accounting for disordered organization of the young fiber cells in the absence of Tmod1.

Next, we wondered whether increasing Tmod1 levels on membranes might be reflected in changes in F-actin organization on the fiber cell membranes as cells matured and moved inward. To test this, we examined the F-actin distribution at the transition from the outer region to the inner region in *Tmod1*+/+$^{Tg+}$ lenses (i.e., where Tmod1 levels increase at ~40 to 50 μm from the epithelium; Fig. 5A, arrow; Fig. 5G, arrow). In Figure 5G–J, a confocal stack is reconstructed to form a three-dimensional image and then tilted to reveal the broad sides of the fiber cell membranes. Strikingly, the F-actin distribution along the fiber cell membranes appears discontinuous in the younger fiber cells but tends to appear smooth and uniform in somewhat older fiber cells, coinciding with the increased levels of Tmod1 on the membranes (Fig. 5G–J). This suggests that enhanced stabilization of F-actin by increased Tmod1 in maturing fiber cells may help prevent the propagation of fiber cell disorder and the larger sized patches observed in the inner region in the absence of Tmod1 (Fig. 4H,I). On the other hand, in *Tmod1*+/+$^{Tg+}$ lenses, the increased Tmod1 does not appear to prevent more small disordered patches from forming as fiber cells mature (Fig. 4H).

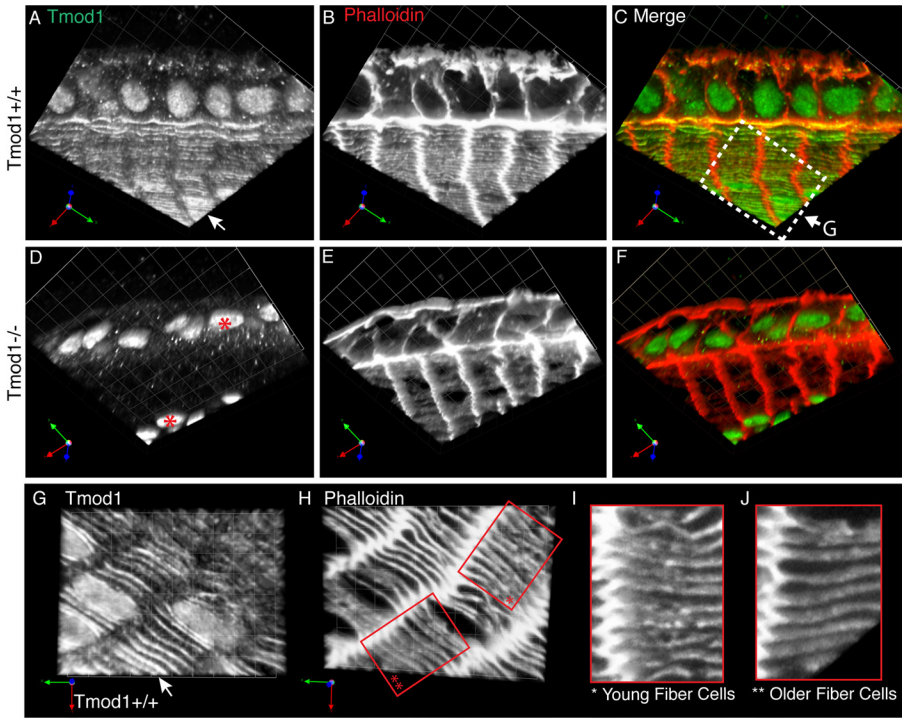

Figure 5. (A–F) Tmod1 assembles on the broad sides of young fiber cells adjacent to the equatorial epithelium. Three-dimensional images of Z stacks of the equatorial epithelium and underlying fiber cells showing Tmod1 (A, D) or F-actin (B, E) in matched regions of mid-equatorial sections of 1-month-old (A–C) *Tmod1*+/+$^{Tg+}$ and (D–F) *Tmod1*–/–$^{Tg+}$ lenses. Merge shown in C, F. Arrows, broad sides. Asterisks, nonspecific nuclear staining for Tmod1 in *Tmod1*–/–$^{Tg+}$ lens. Region delineated by dotted white box in C cropped and enlarged for G, H. (G–I) Increased Tmod1 is associated with acquisition of a uniform F-actin distribution along fiber cell membranes. Three-dimensional images of Z stacks of fiber cells at the transition between low and high Tmod1 staining in a mid-equatorial section of a 1-month-old *Tmod1*+/+$^{Tg+}$ lens, showing (G) increasing Tmod1 levels and (H) F-actin distribution changes. Higher magnification three-dimensional images from red boxes in H, showing fiber cells with (I) lower Tmod1 (younger fiber cells) or (J) higher Tmod1 levels (older fiber cells), tilted to reveal the broad sides of the fiber cells. (A–F) Grid box, 4.6 μm on a side. (G, H) Grid box, 2.6 μm on a side.

Discussion

The hexagonal geometry of lens fiber cells is a beautiful example of long-range cellular order that provides a structural basis for lens transparency. The spectrin-actin network plays an important role in lens fiber cell shape and organization (Nowak et al. 2009), analogous to its role in controlling membrane stability and cell shapes in other cells and tissues (Mohandas and Evans 1994; Bennett and Baines 2001; Thomas 2001). This functionality of the spectrin-actin network is conferred by its long-range connectivity, which depends on F-actin linkers stabilized by the actin-capping proteins, adducin and Tmod1, in association with tropomyosin (Weber KL et al. 2007; Abdi and Bennett 2008; Moyer et al. 2010). Thus, absence of Tmod1 in the lens leads to F-actin depolymerization, loss of tropomyosin (γTM), and disruption of the spectrin-actin network, accompanied by defects in fiber cell shape and organization characterized by disturbance of hexagonal packing geometry (Nowak et al. 2009). An unexpected feature of the *Tmod1*–/–$^{Tg+}$ lens phenotype was the observation that abnormal fiber cell shapes and disordered packing appeared in a patchy fashion in the lens cortex, yet the spectrin-actin network was disrupted in all fiber cells. However, our previous study did not exclude the possibility that subtle changes in cell shape and packing may have been present in other apparently ordered regions or address a cellular mechanism for the appearance of disordered patches. Here, we applied quantitative image analysis and computational approaches to show 1) loss of fiber cell hexagonal packing geometry is confined to focal areas and is not a global feature of the *Tmod1*–/–$^{Tg+}$ lens cortex, 2) fiber cell disorder is not apparent in the meridional rows of differentiating lens epithelial cells at the equator but rather appears first in young elongating fiber cells beneath the equatorial epithelium, and 3) fiber cell disorder appears to propagate by recruitment of additional fiber cells and expansion of disordered patch size during fiber cell maturation in the *Tmod1*–/–$^{Tg+}$ lens cortex. We speculate that abnormal shapes and packing defects in young fiber cells may result from impaired coordination of cell elongation and tip migration due to weakened cell-cell interactions resulting from a disrupted spectrin-actin network in the absence of Tmod1 (Fig. 6A,B). Then, the expansion of disordered areas as fiber cells move inward may result from the inability of a disrupted and attenuated spectrin-actin network to protect against mechanical stresses, resulting in fiber cell rearrangements during lens growth in the absence of Tmod1 (Fig. 6C).

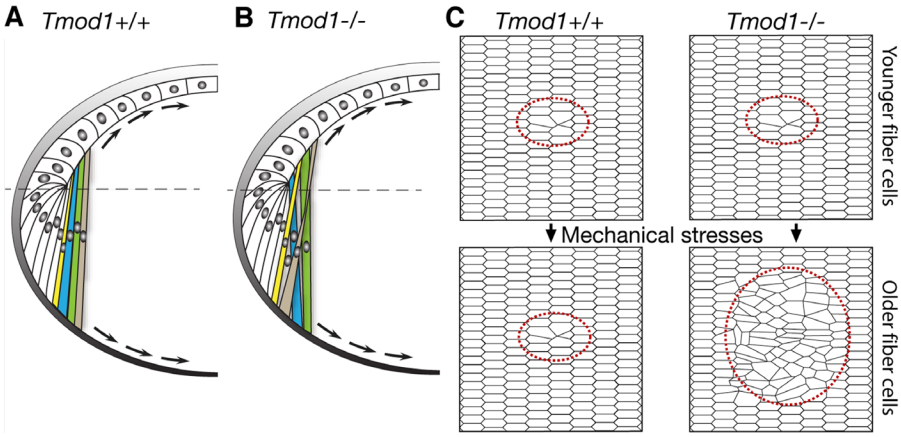

Figure 6. (A, B) Model for generation of disordered fiber cell geometries during cell elongation and migration in *Tmod1*–/–$^{Tg+}$ lenses. (A) Fiber cell interactions in *Tmod1*+/+$^{Tg+}$ lenses may be maintained by an intact spectrin-actin network to promote coherent elongation of fiber cell tips toward the poles. (B) Disordered fiber cell geometry in *Tmod1*–/–$^{Tg+}$ lenses may be due to weakened cell-cell interactions in the presence of a disrupted spectrin-actin network. This could lead to uncoordinated migration rates of adjacent fiber cell tips, leading to mispositioning of adjacent cells along the epithelium or capsule as they elongate and migrate toward the poles. Directions of fiber cell tip migration indicated by arrows. Dotted gray lines indicate plane of section for fiber cells in C. (C) Model for enlargement of disordered patches in *Tmod1*–/–$^{Tg+}$ but not *Tmod1*+/+$^{Tg+}$ lenses. Small packing irregularities exist in both *Tmod1*–/–$^{Tg+}$ and *Tmod1*+/+$^{Tg+}$ lenses but could expand gradually in *Tmod1*–/–$^{Tg+}$ lenses by recruitment of adjacent fiber cells. A disrupted and irregular spectrin-actin network in the absence of Tmod1 with weakened cell-cell interactions could propagate and amplify a non-uniform distribution of stresses on membranes as lens fiber cells mature, resulting in larger areas of abnormal cell shapes and packing geometry. Non-uniform stresses in lens fiber cells may result from extrinsic forces imposed on the lens (tension applied by extraocular muscles) or from internal osmotic forces (radial solute gradients), which depend on the location of the fiber cells in the lens.

How does the appearance of focal defects in fiber cell packing geometry in *Tmod1*–/–$^{Tg+}$ lenses relate to Tmod1 expression and membrane association? *Tmod1* mRNA expression in the mouse is initiated as epithelial cells differentiate to fiber cells at the lens equator (Sussman et al. 1996). However, Tmod1 protein staining is first detected in association with fiber cell membranes in the elongating fiber cells adjacent to the equatorial epithelium (this study, Fig. 5). Similarly, in the chicken lens where Tmod4 is expressed instead of Tmod1 (Almenar-Queralt et al. 1999; Fischer et al. 2000), Tmod4 expression is initiated upon fiber cell differentiation (Fischer et al. 2000), with diffuse staining detected in the annular pad region where the epithelial cells begin to elongate to form fiber cells (Lee et al. 2000). Tmod4 then assembles on membranes after fiber cells "round the bend" and begin to elongate and migrate with their tips oriented toward the poles (Lee et al. 2000). Thus, the appearance of focal areas of disordered packing in young fiber cells in *Tmod1*–/–$^{Tg+}$ mouse lenses coincides with the timing of Tmod1's association with membranes during fiber cell elongation and migration in *Tmod1*+/+$^{Tg+}$ lenses. By contrast, although Tmod1 may be present at low levels in differentiating epithelial cells, it is not required for the epithelial cell polarization and rearrangement events to form the meridional rows at the equator.

What could account for a Tmod1 requirement in the dynamic events of fiber cell morphogenesis encompassing cell tip migration and elongation toward the poles? Two possible mechanisms come to mind. First, a Tmod1-stablized spectrin-actin network linked to adhesion receptors (e.g., NrCAM, N-cadherin) (More et al. 2001; Straub et al. 2003; Nowak et al. 2009) may be required to maintain correct fiber cell interactions with their neighboring cells in the same and adjacent fiber cell layers (shells) (Fig. 6A,B). If cell-cell interactions between Tmod1-null cells are weakened, then the tips of adjacent fiber cells could migrate at different rates. Over time, such uncoordinated migration could result in adjacent fiber cell tips being located at different positions along the surface of the epithelium or capsule as the cells elongate toward the poles. In cross sections, such misalignments of adjacent cells would appear as a disturbance of hexagonal packing geometry. Consistent with this idea, F-actin staining on broad sides of young fiber cells of *Tmod1*–/–$^{Tg+}$ lenses appears depleted as compared with *Tmod1*+/+$^{Tg+}$ lenses (compare Fig. 5B with 5E), which may lead to weaker spectrin-actin associations with membrane receptors, with consequent cell slippage and incoherent migration. However, it is notable that in *Tmod1*+/+$^{Tg+}$ lenses, F-actin staining on membranes of young fiber cells with low levels of Tmod1 is not uniform and continuous, as compared with older fiber cells with higher levels of Tmod1 (Fig. 5G–I) (Nowak et al. 2009). Indeed the discontinuous, non-uniform F-actin distribution on membranes of young fiber cells with low levels of Tmod1 resembles the disrupted F-actin staining on membranes of fiber cells without Tmod1, in *Tmod1*–/–$^{Tg+}$ lenses (Nowak et al. 2009). Therefore, in an alternative interpretation, it may be that absence of Tmod1 leads to an attempt to compensate by upregulation of another Tmod isoform, which itself leads to abnormal cellular shapes and interactions with misregulated

migration via a gain-of-function mechanism. For example, in *Tmod1–/–*$^{Tg+}$ skeletal muscle and erythrocytes, ineffective compensation by Tmod3 leads to abnormal F-actin organization and cell physiology (Gokhin et al. 2010; Moyer et al. 2010; Gokhin and Fowler 2011). In this context, it is significant that Tmod3 has been shown to regulate cell migration of human microvascular endothelial cells in vitro (Fischer, Fritz-Six, et al. 2003). The expression of other Tmod isoforms in the lens remains to be studied.

What might explain the expanded sizes of disordered regions as fiber cells mature in the Tmod1-null lens cortex? In *Tmod1+/+*$^{Tg+}$ lenses, the amount of Tmod1 associated with fiber cell membranes increases dramatically as fiber cells mature and move inward (Nowak et al. 2009) (Figs. 4 and 5, this study). Concomitant with the increase in Tmod1, F-actin staining on fiber cell membranes becomes denser and more uniformly distributed, suggesting fortification of the spectrin-actin network by more F-actin linkers capped by Tmod1. Thus, the location of increased Tmod1 levels and more uniform F-actin distribution on membranes in *Tmod1+/+*$^{Tg+}$ lenses correlates with the location of larger disordered patches in *Tmod1–/–*$^{Tg+}$ lenses, providing a direct link between Tmod1, F-actin, and the *Tmod1–/–*$^{Tg+}$ phenotype. Yet, although loss of Tmod1 leads to F-actin disruption in all fiber cells, all fiber cells do not become disordered as they mature and move inward in the lens cortex.

The following observations provide clues to a possible mechanism. First, nearest neighbor analysis of fiber cell geometry shows that decreased hexagonal packing is restricted to localized patches in the lens cortex (Figs. 1 and 2). This indicates that the appearance of larger disordered patches during lens fiber cell maturation in the absence of Tmod1 is not accompanied by a global loss of hexagonal packing throughout the cortex. Second, the numbers of disordered patches are greater for older fiber cells than for younger fiber cells in *Tmod1+/+*$^{Tg+}$, evidencing an unanticipated dynamism in lens fiber cell hexagonal packing, which is up to now not described in the literature. Third, areas of individual disordered patches of older fiber cells in *Tmod1–/–*$^{Tg+}$ lenses are larger than in *Tmod1+/+*$^{Tg+}$ lenses (Fig. 4). Such a localized phenomenon suggests that large patches in deeper regions of the cortex are due to propagation of a local packing defect by recruitment of additional fiber cells at the periphery of disordered patches in the absence, but not presence, of Tmod1.

Therefore, we propose a mechanism based on a non-uniform distribution of mechanical stresses in the lens to account for increased fiber cell disorder as fiber cells mature in *Tmod1–/–*$^{Tg+}$ lenses, which is illustrated in Figure 6C. In an ideal hexagonally packed array of identical cells, mechanical stresses are automatically evenly distributed along all cell membranes (Carthew 2005; Lecuit and Lenne 2007). If irregularities are present, such as at sites of the small packing imperfections observed in *Tmod1+/+*$^{Tg+}$ and *Tmod1–/–*$^{Tg+}$ lenses alike, local stress gradients and peaks are a necessary consequence. However, in the absence of Tmod1, imbalanced stresses may be further propagated and amplified due to the irregular and disrupted spectrin-actin network organization. This could then lead to further membrane deformations and abnormal cell shapes, similar to the well-documented effects of mechanical stresses on erythrocytes with a defective and attenuated spectrin-actin network (Mohandas and Evans 1994; Mohandas and Gallagher 2008). In other epithelial systems, non-uniform stress distributions have been shown to perturb cell-cell junction organization and lead to membrane deformations, cell rearrangements, and loss of hexagonal packing geometry (Blankenship et al. 2006; Farhadifar et al. 2007; Montell 2008; Rauzi et al. 2008). Thus, small patches of a few non-hexagonally packed cells may increase in size under the influence of non-uniform mechanical stresses when the underlying spectrin-actin network is disrupted and cell-cell interactions are weakened, allowing cellular rearrangements (Fig. 6C).

What might be the source of non-uniform distributions of mechanical stresses in the lens? First, extraocular muscles pulling on the lens apply tensile forces extrinsic to the lens itself, which are expected to lead to non-uniform stresses within the lens due to Poisson's ratio effects. This is because for objects with complex geometries and non-uniform densities (such as the lens and most biological tissues), Poisson's ratios would be expected to vary throughout the object as a function of spatial position, leading to complex force and deformation gradients (which have not yet been described for the lens) (Fung 1993). Second, the lens ionic circulation system creates a radial gradient of solutes and hydrostatic pressure in fiber cells that increases toward the center of the lens (Mathias et al. 2010). Increasing solute concentrations result in increasing levels of osmotic pressure experienced by fiber cells as they move inward in the lens cortex, thereby increasing the physical stresses on their membranes.

Our data are thus consistent with the notion that the spectrin-actin network functions to distribute stresses evenly across the fiber cell membranes and from cell to cell, both during coordinated fiber cell elongation toward the poles and, subsequently, during fiber cell maturation. Disruption in this network upon loss of Tmod1, leading to irregular F-actin distribution, would then result in an imbalance of forces leading to fiber cell rearrangements and disordered geometries. Fiber cell interactions may be most sensitive to loss of Tmod1 during fiber cell elongation and migration, explaining the de novo appearance of focal packing defects in young fiber cells in the absence but not the presence of Tmod1. On the other hand, stresses on maturing fiber cells that move inward during lens growth may lead to local fiber cell rearrangements even with an intact spectrin-actin network (in the presence of

Tmod1), yet the absence of Tmod1 would exacerbate the irregular distribution of forces, thereby resulting in expanded regions of disorder. Presumably, forces are transmitted from the spectrin-actin network to the cell membrane via network linkages to membrane proteins such as N-cadherin (Straub et al. 2003), NrCAM (More et al. 2001), or other receptors. Alternatively, it is conceivable that Tmod1 itself may directly link F-actin in the spectrin-actin network to membrane proteins, but this has not been investigated.

Abnormal fiber cell shapes and qualitative loss of hexagonal packing geometry have also been observed in lenses from mice with targeted deletions in the axon guidance molecules, ephrin-A5 ligand (Cooper et al. 2008) and EPHA2 receptor (Jun et al. 2009), the beaded filament proteins, CP49 and filensin (Sandilands et al. 2003; Yoon et al. 2008), and the cytoskeletal scaffolding protein, periaxin (Maddala et al. 2011). In the case of ephrin-A5- or EPHA2-null mice, abnormal fiber cell shapes and disordered packing are evident in young fiber cells likely still in the process of elongation, similar to Tmod1-null lenses (Cooper et al. 2008; Jun et al. 2009). In contrast, in the case of beaded filament-null lenses, abnormal shapes and disorder are reported in the deep cortex (Sandilands et al. 2003; Yoon et al. 2008). In the periaxin-deficient lenses, the location of fiber cell disorder is also likely to be the inner cortical fiber cells (Maddala et al. 2011). However, with the exception of our study here on Tmod1-null lenses, shapes and packing of younger and older fiber cells were not compared directly, and a systematic analysis of the extent of fiber cell disorder with respect to the stages of lens epithelial cell differentiation, fiber cell elongation, and maturation has not been attempted. Thus, it is not clear whether the disordered fiber cells in the peripheral cortex of the ephrin-A5-null or EPHA2-null lenses arise due to defects in epithelial differentiation and initial establishment of meridional rows at the equator or subsequently due to defects in the elongation and migration of fiber cells and/or whether the disorder worsens with fiber cell maturation in the cortex. Conversely, it is not known whether abnormal fiber cell geometry in the deep cortex of beaded filament-null lenses might be presaged by small focal regions of disorder located more peripherally in the cortex. Indeed, we observed that the number of small packing imperfections was greater in older as compared with younger fiber cells in our control lenses (Fig. 4H), which contain Tmod1 but are missing beaded filaments, due to an endogenous mutation in CP49 (Nowak et al. 2009).

Absence of beaded filaments has been shown previously to impair maintenance of the elaborate interlocking membrane protrusions (termed *hands*) between fiber cells in the inner cortex, likely interfering with fiber cell interactions and leading to disordered cell packing (Sandilands et al. 2003; Blankenship et al. 2007; Yoon et al. 2008). Thus, the magnitude of abnormal membrane morphologies and cell disorder due to a disrupted spectrin-actin network in the absence of Tmod1 (Nowak et al. 2009) may be masked by the effects of the concomitant absence of beaded filaments. Alternatively, the beaded filaments and spectrin-actin filament networks could be interconnected, and the perturbations observed in Tmod1/CP49-null lenses could be due to Tmod1 deletion potentiating the effects of beaded filament deletion. Indeed, direct connections between the actin and beaded filament systems are suggested by our previous study showing that Tmod4 in the chicken lens binds directly to filensin (Fischer, Quinlan, et al. 2003). Future studies comparing fiber cell disorder in lenses with and without beaded filaments, or in lenses missing Tmod1 but not beaded filaments, will be required to address this question.

It is likely that phenotypes characterized by loss of fiber cell hexagonal shape and disordered packing geometry will fall into three broad categories: those arising from defects in epithelial cell differentiation and initial establishment of meridional rows at the equator, those arising from defective spatial and temporal coordination of elongation and migration of fiber cell tips, and those arising from inability to maintain fiber cell packing geometries during subsequent maturation as fiber cells move inward. The methodology we have developed will allow us and other investigators to begin to systematically analyze the various mouse knockout lens phenotypes to answer these questions.

Acknowledgements

We thank Martin Dressler for initiating this study and for his substantial contributions to the experiments and text of the manuscript. His work was performed in partial fulfillment of a master's thesis at the Ecole Superieure de Biotechnologie de Strasbourg, France, 2009. We thank David Gokhin for help with statistical analysis and Bill Kiosses for help with confocal microscopy.

Declaration of Conflicting Interests

The authors declared no potential conflicts of interest with respect to the research, authorship, and/or publication of this article.

Funding

The authors disclosed receipt of the following financial support for the research, authorship, and/or publication of this article: This work was supported by grant EY017724 from the National Institutes of Health (National Eye Institute) to V.M.F.

References

Abdi KM, Bennett V. 2008. Adducin promotes micrometer-scale organization of beta2-spectrin in lateral membranes of bronchial epithelial cells. Mol Biol Cell. 19:536–545.

Almenar-Queralt A, Lee A, Conley CA, Ribas de Pouplana L, Fowler VM. 1999. Identification of a novel tropomodulin isoform, skeletal tropomodulin, that caps actin filament pointed ends in fast skeletal muscle. J Biol Chem. 274:28466–28475.

Bassnett S. 2009. On the mechanism of organelle degradation in the vertebrate lens. Exp Eye Res. 88:133–139.

Bassnett S, Winzenburger PA. 2003. Morphometric analysis of fibre cell growth in the developing chicken lens. Exp Eye Res. 76:291–302.

Bennett V, Baines AJ. 2001. Spectrin and ankyrin-based pathways: metazoan inventions for integrating cells into tissues. Physiol Rev. 81:1353–1392.

Bennett V, Healy J. 2008. Organizing the fluid membrane bilayer: diseases linked to spectrin and ankyrin. Trends Mol Med. 14:28–36.

Blankenship JT, Backovic ST, Sanny JS, Weitz O, Zallen JA. 2006. Multicellular rosette formation links planar cell polarity to tissue morphogenesis. Dev Cell. 11:459–470.

Blankenship T, Bradshaw L, Shibata B, Fitzgerald P. 2007. Structural specializations emerging late in mouse lens fiber cell differentiation. Invest Ophthalmol Vis Sci. 48:3269–3276.

Carthew RW. 2005. Adhesion proteins and the control of cell shape. Curr Opin Genet Dev. 15:358–363.

Classen AK, Anderson KI, Marois E, Eaton S. 2005. Hexagonal packing of *Drosophila* wing epithelial cells by the planar cell polarity pathway. Dev Cell. 9:805–817.

Cooper MA, Son AI, Komlos D, Sun Y, Kleiman NJ, Zhou R. 2008. Loss of ephrin-A5 function disrupts lens fiber cell packing and leads to cataract. Proc Natl Acad Sci U S A. 105:16620–16625.

Dubreuil RR. 2006. Functional links between membrane transport and the spectrin cytoskeleton. J Membr Biol. 211:151–161.

Farhadifar R, Roper JC, Aigouy B, Eaton S, Julicher F. 2007. The influence of cell mechanics, cell-cell interactions, and proliferation on epithelial packing. Curr Biol. 17:2095–2104.

Fischer RS, Fritz-Six KL, Fowler VM. 2003. Pointed-end capping by tropomodulin3 negatively regulates endothelial cell motility. J Cell Biol. 161:371–380.

Fischer RS, Lee A, Fowler VM. 2000. Tropomodulin and tropomyosin mediate lens cell actin cytoskeleton reorganization in vitro. Invest Ophthalmol Vis Sci. 41:166–174.

Fischer RS, Quinlan RA, Fowler VM. 2003. Tropomodulin binds to filensin intermediate filaments. FEBS Lett. 547:228–232.

Fowler VM. 1987. Identification and purification of a novel Mr 43,000 tropomyosin-binding protein from human erythrocyte membranes. J Biol Chem. 262:12792–12800.

Fowler VM. 1996. Regulation of actin filament length in erythrocytes and striated muscle. Curr Opin Cell Biol. 8:86–96.

Fowler VM, Bennett V. 1984. Erythrocyte membrane tropomyosin: purification and properties. J Biol Chem. 259:5978–5989.

Fritz-Six KL, Cox PR, Fischer RS, Xu B, Gregorio CC, Zoghbi HY, Fowler VM. 2003. Aberrant myofibril assembly in tropomodulin1 null mice leads to aborted heart development and embryonic lethality. J Cell Biol. 163:1033–1044.

Fung YC. 1993. Biomechanics: mechanical properties of living tissues. 2nd ed. New York: Springer.

Gibson MC, Patel AB, Nagpal R, Perrimon N. 2006. The emergence of geometric order in proliferating metazoan epithelia. Nature. 442:1038–1041.

Gilligan DM, Bennett V. 1993. The junctional complex of the membrane skeleton. Semin Hematol. 30:74–83.

Gokhin DS, Fowler VM. 2011. Cytoplasmic gamma-actin and tropomodulin isoforms link to the sarcoplasmic reticulum in skeletal muscle fibers. J Cell Biol. 194:105–120.

Gokhin DS, Lewis RA, McKeown CR, Nowak RB, Kim NE, Littlefield RS, Lieber RL, Fowler VM. 2010. Tropomodulin isoforms regulate thin filament pointed-end capping and skeletal muscle physiology. J Cell Biol. 189:95–109.

Jun G, Guo H, Klein BE, Klein R, Wang JJ, Mitchell P, Miao H, Lee KE, Joshi T, Buck M, et al. 2009. EPHA2 is associated with age-related cortical cataract in mice and humans. PLoS Genet. 5:e1000584.

Kizhatil K, Bennett V. 2004. Lateral membrane biogenesis in human bronchial epithelial cells requires 190-kDa ankyrin-G. J Biol Chem. 279:16706–16714.

Kizhatil K, Davis JQ, Davis L, Hoffman J, Hogan BL, Bennett V. 2007. Ankyrin-G is a molecular partner of E-cadherin in epithelial cells and early embryos. J Biol Chem. 282:26552–26561.

Kizhatil K, Yoon W, Mohler PJ, Davis LH, Hoffman JA, Bennett V. 2007. Ankyrin-G and beta2-spectrin collaborate in biogenesis of lateral membrane of human bronchial epithelial cells. J Biol Chem. 282:2029–2037.

Kuhlman PA, Hughes CA, Bennett V, Fowler VM. 1996. A new function for adducin: calcium/calmodulin-regulated capping of the barbed ends of actin filaments. J Biol Chem. 271:7986–7991.

Kuszak JR. 1995. The ultrastructure of epithelial and fiber cells in the crystalline lens. Int Rev Cytol. 163:305–350.

Kuszak JR, Zoltoski RK, Sivertson C. 2004. Fibre cell organization in crystalline lenses. Exp Eye Res. 78:673–687.

Lecuit T, Lenne PF. 2007. Cell surface mechanics and the control of cell shape, tissue patterns and morphogenesis. Nat Rev Mol Cell Biol. 8:633–644.

Lee A, Fischer RS, Fowler VM. 2000. Stabilization and remodeling of the membrane skeleton during lens fiber cell differentiation and maturation. Dev Dyn. 217:257–270.

Lovicu FJ, Robinson ML. 2004. Development of the ocular lens. Cambridge, UK: Cambridge University Press.

Luna EJ, Hitt AL. 1992. Cytoskeleton-plasma membrane interactions. Science. 258:955–964.

Maddala R, Skiba NP, Lalane R III, Sherman DL, Brophy PJ, Rao PV. 2011. Periaxin is required for hexagonal geometry and membrane organization of mature lens fibers. Dev Biol. 357:179–190.

Maisel H, Harding CV, Alcala JR, Kuszak J, Bradley R. 1981. The morphology of the lens. In: Bloemendal H, editor. Molecular and cell biology of the eye lens. New York: John Wiley. p. 49–84.

Mathias RT, White TW, Gong X. 2010. Lens gap junctions in growth, differentiation, and homeostasis. Physiol Rev. 90:179–206.

McKeown CR, Nowak RB, Moyer J, Sussman MA, Fowler VM. 2008. Tropomodulin1 is required in the heart but not the yolk sac for mouse embryonic development. Circ Res. 103:1241–1248.

Mohandas N, Evans E. 1994. Mechanical properties of the red cell membrane in relation to molecular structure and genetic defects. Annu Rev Biophys Biomol Struct. 23:787–818.

Mohandas N, Gallagher PG. 2008. Red cell membrane: past, present, and future. Blood. 112:3939–3948.

Montell DJ. 2008. Morphogenetic cell movements: diversity from modular mechanical properties. Science. 322:1502–1505.

More MI, Kirsch FP, Rathjen FG. 2001. Targeted ablation of NrCAM or ankyrin-B results in disorganized lens fibers leading to cataract formation. J Cell Biol. 154:187–196.

Moyer JD, Nowak RB, Kim NE, Larkin SK, Peters LL, Hartwig J, Kuypers FA, Fowler VM. 2010. Tropomodulin 1-null mice have a mild spherocytic elliptocytosis with appearance of tropomodulin 3 in red blood cells and disruption of the membrane skeleton. Blood. 116:2590–2599.

Nowak RB, Fischer RS, Zoltoski RK, Kuszak JR, Fowler VM. 2009. Tropomodulin1 is required for membrane skeleton organization and hexagonal geometry of fiber cells in the mouse lens. J Cell Biol. 186:915–928.

Rauzi M, Verant P, Lecuit T, Lenne PF. 2008. Nature and anisotropy of cortical forces orienting *Drosophila* tissue morphogenesis. Nat Cell Biol. 10:1401–1410.

Sandilands A, Prescott AR, Wegener A, Zoltoski RK, Hutcheson AM, Masaki S, Kuszak JR, Quinlan RA. 2003. Knockout of the intermediate filament protein CP49 destabilises the lens fibre cell cytoskeleton and decreases lens optical quality, but does not induce cataract. Exp Eye Res. 76:385–391.

Shi Y, Barton K, De Maria A, Petrash JM, Shiels A, Bassnett S. 2009. The stratified syncytium of the vertebrate lens. J Cell Sci. 122:1607–1615.

Shui YB, Beebe DC. 2008. Age-dependent control of lens growth by hypoxia. Invest Ophthalmol Vis Sci. 49:1023–1029.

Simirskii VN, Lee RS, Wawrousek EF, Duncan MK. 2006. Inbred FVB/N mice are mutant at the cp49/Bfsp2 locus and lack beaded filament proteins in the lens. Invest Ophthalmol Vis Sci. 47:4931–4934.

Straub BK, Boda J, Kuhn C, Schnoelzer M, Korf U, Kempf T, Spring H, Hatzfeld M, Franke WW. 2003. A novel cell-cell junction system: the cortex adhaerens mosaic of lens fiber cells. J Cell Sci. 116:4985–4995.

Sussman MA, McAvoy JW, Rudisill M, Swanson B, Lyons GE, Kedes L, Blanks J. 1996. Lens tropomodulin: developmental expression during differentiation. Exp Eye Res. 63:223–232.

Sussman MA, Welch S, Cambon N, Klevitsky R, Hewett TE, Price R, Witt SA, Kimball TR. 1998. Myofibril degeneration caused by tropomodulin overexpression leads to dilated cardiomyopathy in juvenile mice. J Clin Invest. 101:51–61.

Tardieu A. 1988. Eye lens proteins and transparency: from light transmission theory to solution X-ray structural analysis. Annu Rev Biophys Biophys Chem. 17:47–70.

Thomas GH. 2001. Spectrin: the ghost in the machine. Bioessays. 23:152–160.

Weber A, Pennise CR, Babcock GG, Fowler VM. 1994. Tropomodulin caps the pointed ends of actin filaments. J Cell Biol. 126(Pt. 1):1627–1635.

Weber KL, Fischer RS, Fowler VM. 2007. Tmod3 regulates polarized epithelial cell morphology. J Cell Sci. 120:3625–3632.

Yoon KH, Blankenship T, Shibata B, Fitzgerald PG. 2008. Resisting the effects of aging: a function for the fiber cell beaded filament. Invest Ophthalmol Vis Sci. 49:1030–1036.